

Radiometric sand–mud characterisation in the Rhine–Meuse estuary Part A. Fingerprinting

M. van Wijngaarden^{a,*}, L.B. Venema^b, R.J. De Meijer^b, J.J.G. Zwolsman^a,
B. Van Os^c, J.M.J. Gieske^c

^aMinistry of Transport, Public Works and Water Management, Institute for Inland Water Management and Waste Water Treatment (RIZA),
P.O. Box 52, 3300 AB Dordrecht, The Netherlands

^bNuclear Geophysics Division, Kernfysisch Versneller Instituut, University Groningen, Zernikelaan 25, 9747 AA Groningen,
The Netherlands

^cInstitute for Applied Geosciences, NITG-TNO, P.O. Box 80015, 3508 TA Utrecht, The Netherlands

Received 26 February 2001; received in revised form 14 July 2001; accepted 22 July 2001

Abstract

The composition of the underwater sediment bed is often defined in terms of the mud (<63 µm) or sand (>63 and <2000 µm) content. Mud and sand differ considerably in their content of (natural) radionuclides. Radionuclide concentrations are highest in the clay minerals that form a significant part of the mud fraction. A study was initiated in the Hollandsch Diep and Haringvliet, two semi-stagnant fresh water basins in the southwestern part of Rhine–Meuse Estuary (The Netherlands), to investigate whether radionuclides can be utilised to determine the sand and mud content of aquatic sediments. The radiometric fingerprint was assessed based on sediment samples with different composition, provenance and age. Differences in provenance (Rhine versus Meuse) could be discriminated by the ⁴⁰K content of the sediment. Differences in age or composition, in terms of mineralogy, organic matter or carbonate content, only slightly affected the radiometric characteristics based on ²³²Th and ²³⁸U. On the other hand, no reliable correlation between ⁴⁰K and the mud content was obtained; therefore, ⁴⁰K is excluded from the fingerprint. The fingerprints based on the ²³²Th and ²³⁸U contents characterise mud (<63 µm) and sand (>63 µm) as: 46.2 ± 1.9 Bq/kg ²³⁸U and 9.3 ± 0.9 Bq/kg ²³⁸U and 45.6 ± 1.9 Bq/kg ²³²Th and 9.7 ± 0.9 Bq/kg ²³²Th, respectively. The assessed radiometric fingerprint allows a quantitative interpretation of the mud and sand content through the total ²³⁸U + ²³²Th activity. This interpretation is confirmed by the high correlation ($R^2 = 0.96$) for the mud percentages obtained from radiometric analysis and those by laser diffraction in the laboratory. It can be concluded that radiometric sedimentology provides a tool for reliable sediment characterisation. New perspectives are opened when radiometric fingerprints are combined with in situ radiometric characterisation of sediments, which will be presented in part B of this paper (this issue). © 2002 Elsevier Science B.V. All rights reserved.

Keywords: Sediment composition; Sand–mud ratio; Natural radioactivity; Radiometric fingerprint

* Corresponding author. Fax: +31-78-6315003.

E-mail address: m.vwijngaarden@riza.rws.minvenw.nl (M. van Wijngaarden).

1. Introduction

The composition of a natural sediment bed is the result of various morphodynamic processes and can be characterised by its sand (>63 and <2000 μm) and clay (<2 μm), silt (<16 μm) or mud content (<63 μm). Especially in delta systems where the deposition or erosion of mud and sand occurs under specific (tidal) conditions, such a classification appears often to be more functional than grain-size information expressed by a median diameter. The sand or mud content provides information with respect to (a) the sediment-transport processes active in a water system and (b) the (potential) degree of pollution of the sediments, which is strongly correlated to the mud content (Horowitz and Elrick, 1987; Zwolsman et al., 1996).

Sand and mud have different geochemical and physical properties and are transported in a different manner. Sand is an inorganic, silicium-rich coarse material, which is transported mainly as bedload. Mud is a fine, cohesive material, still rich in silicium, quartz and feldspars, but also in organic matter and clay minerals and is transported in suspension. Al_2O_3 is a main constituent of these clay minerals. Moreover, clay minerals have a high adsorption potential for trace metals and radionuclides. Studies suggest that as a result of their specific adsorptive behaviour, radio-

nuclides can very well function as indicators for the mud and sand content of submerged sediments (Duursma and Bosch, 1970; Duursma and Eisma, 1973; Venema and De Meijer, 2001).

Most methods used to characterise sediments are laboratory-based, requiring collection of sediment samples from the field. Given the spatial heterogeneity of most natural aquatic sediments, to obtain accurate spatial information, extensive sediment sampling is required which often turns into a costly and time-consuming operation. Therefore, a distinct need for reliable and fast in situ techniques exists, for which radiometric sedimentology is a promising candidate.

In radiometric sedimentology, various sediment components are characterised using the concentration of natural, gamma-ray emitting radionuclides. Three of the main radionuclides in the natural environment, ^{238}U , ^{232}Th and ^{40}K , are generally used as they have a half-life longer or comparable to the earth's existence ($t_{1/2}$ of ^{238}U , ^{232}Th and ^{40}K is 4.5, 14 and 1.3 Ga, respectively). Accordingly, these nuclides form excellent indicators for intrinsic sediment properties. Their presence can be measured through the emission of γ -rays during decay, either directly (^{40}K) or via decay products (^{238}U and ^{232}Th). Such γ -ray activity cannot only be analysed in sediment samples in the laboratory, but also non-invasively and in situ by trailing a γ -ray detector over the sediment bed.

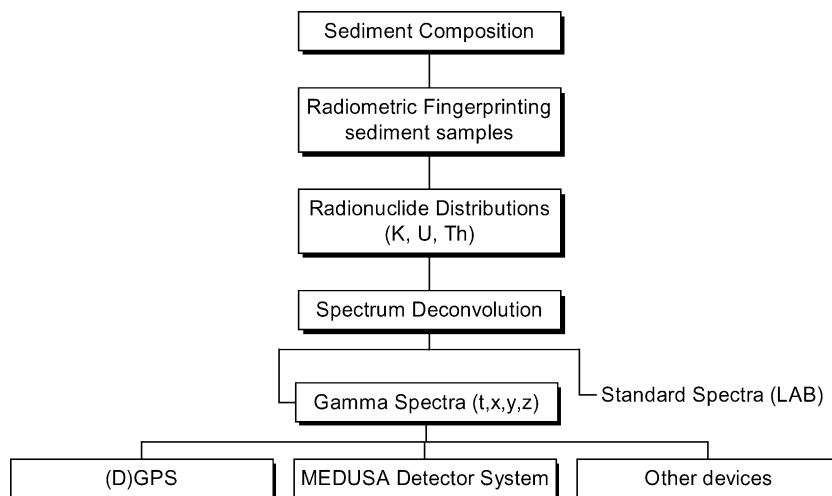


Fig. 1. Schematic outline of the process of radiometric sedimentology.

The methodology used in this paper is schematically presented in Fig. 1. The radiometric characterisation of sediments is conducted in the laboratory, resulting in sediment component-specific radiometric fingerprints. In this study, the radiometric fingerprint of a sediment component is defined as the representative combination of the activity concentration of ^{238}U , ^{232}Th and ^{40}K . Geochemical analyses were used to assess the quality and/or diversity of the samples used for this fingerprint, regarding age, provenance and composition. A radionuclide distribution map is derived from in situ measured γ -ray spectra obtained with the 'Multi-Detector system for Underwater Sediment Activity' (MEDUSA) (Venema and De Meijer, 2001; Hendriks et al., 2001). The

combination results in a map of the sediment composition.

This methodology was put into practice, resulting in a sand–mud map of the aquatic sediments of the Hollandsch Diep and Haringvliet, two semi-stagnant fresh water basins in the southwestern part of Rhine–Meuse Estuary (The Netherlands); see Fig. 2. Since the closure of this former estuary area from the sea in 1970, significant sedimentation of mud has occurred in the tidal channels. The eastern section near the rivers' outflow is well known for its mud deposits several meters thick, whereas the western section has much lower sedimentation rates with mud deposits being more dispersed across the area. As the former estuarine sandy deposits are still present as

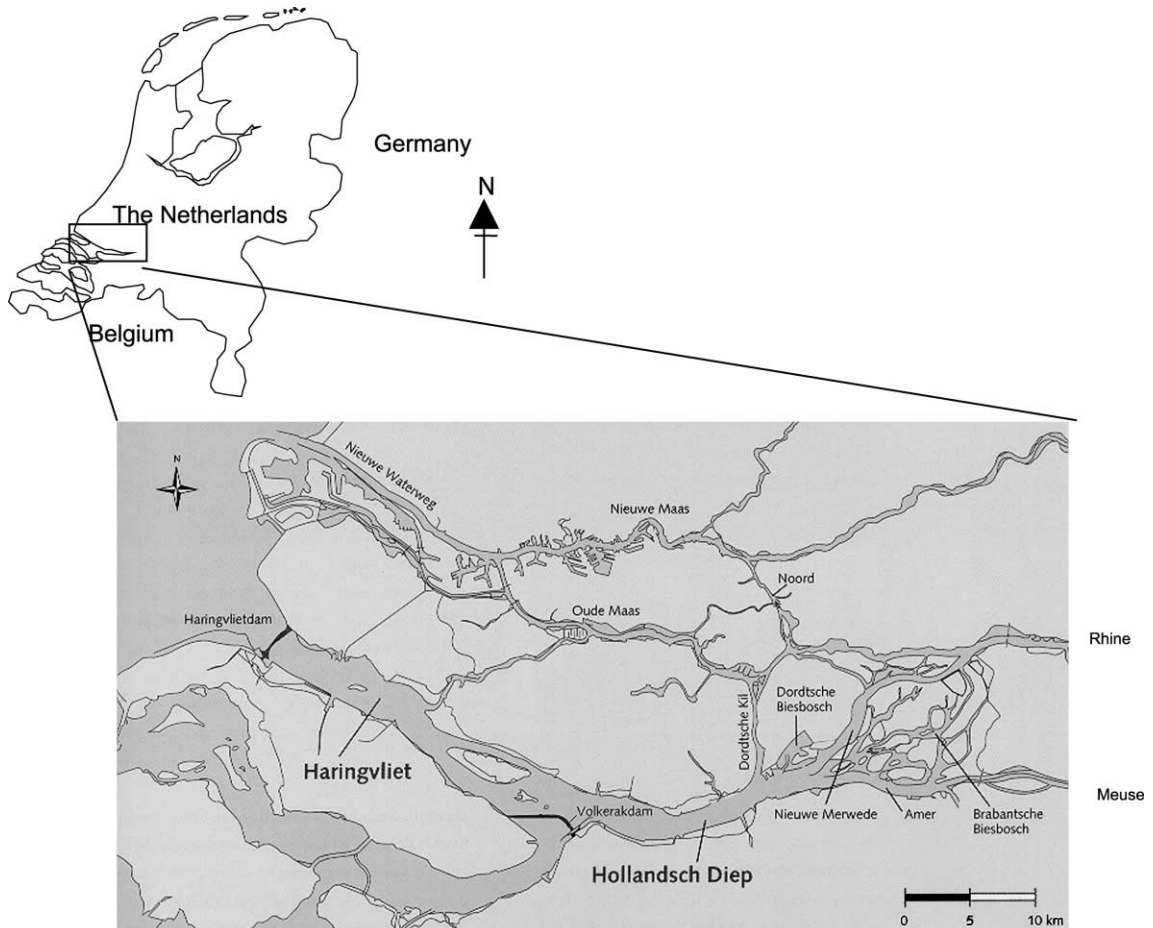


Fig. 2. Layout of the Rhine–Meuse Estuary and location of the study area Hollandsch Diep and Haringvliet.

shallow flats, this area offers a perfect case for using radiometric sedimentology to map the sand mud content.

This paper, part A, describes the derivation of the fingerprints for mud and sand in the Hollandsch Diep and Haringvliet. The implementation of the in situ radiometric technique MEDUSA and the actual derivation of the sand–mud maps will be described in part B of this paper (this issue).

2. Geographical setting

The rivers Rhine and Meuse form a combined estuary in the southwestern part of The Netherlands (Fig. 2). The hydrodynamics of the estuary are highly regulated by control of river inflows and mainte-

nance dredging of shipping channels. The northern outlet of the estuary to the North Sea is via Rotterdam Waterway. The southern part of the estuary consists of two fresh water bodies: the Haringvliet and Hollandsch Diep. After the completion of the Haringvliet Dam in 1970, this southern branch of the estuary changed from a dynamic brackish tidal inlet into a semi-stagnant freshwater area, which had severe effects on the ecological values of the area (Ferguson and Wolff, 1984). Sluices in the dam are operated using a manipulation programme which guarantees a minimum flow (1500 m³/s) through the northern outlet of the estuary, the Rotterdam Waterway, when the Rhine discharge exceeds 1700 m³/s (approximately 60% of the year); the remaining flow is discharged through the Haringvliet during low tide.

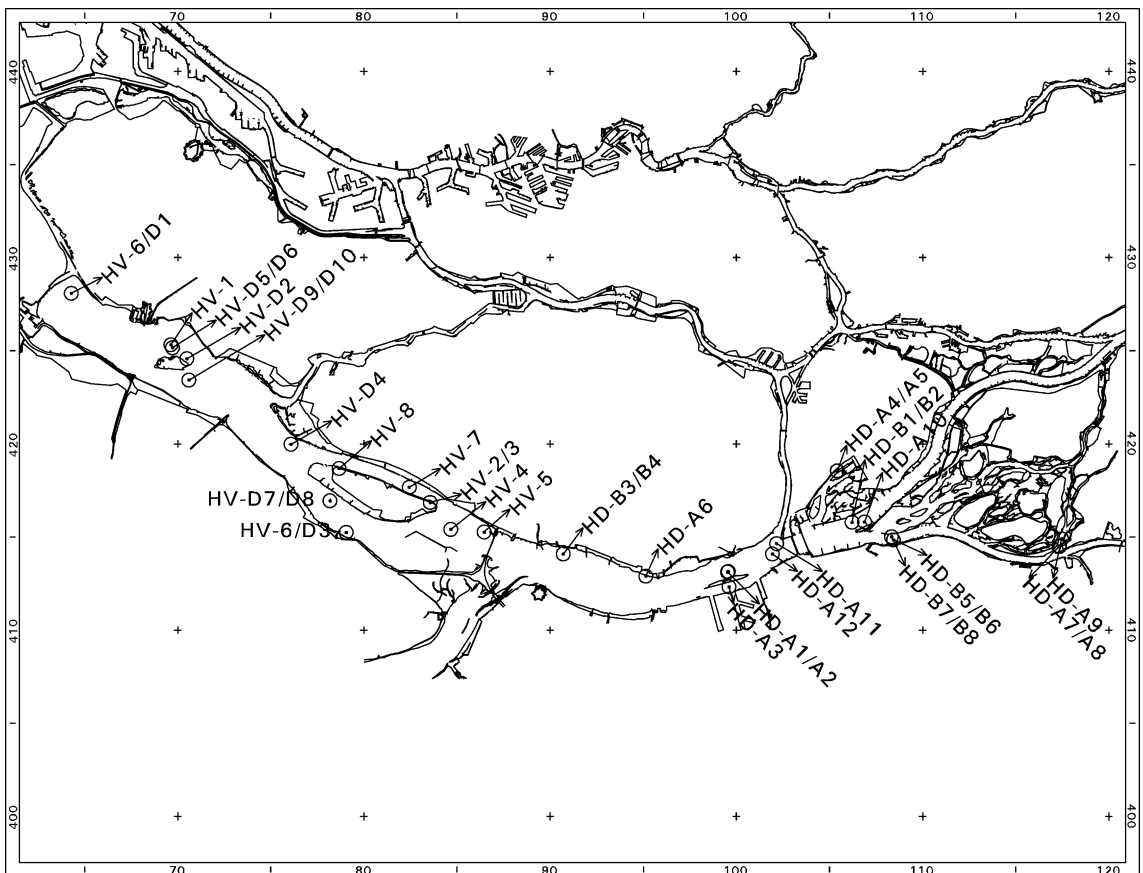


Fig. 3. Sampling locations in the study area.

Due to the construction of the Haringvliet Dam, flow velocities in the inland waters decreased dramatically and, consequently, sedimentation was initiated in the eastern part of the Hollandsch Diep basin. Some 75% of the suspended sediments by the rivers Rhine (1.9 Mton/year) and Meuse (0.3 Mton/year) is deposited in the Hollandsch Diep basin (Van Dreumel, 1995). The sedimentation area has a length of approximately 30 km and a width of 1–4 km. Actual sediment accumulation rates in the Hollandsch Diep range from several centimeters per year for both ends of the basin to 20 cm/year in the central parts (Van Eck et al., 1997). In the Haringvliet sediment, accumulation rates amount to on average 1 cm/year (Van Wijngaarden and Ludikhuizen, 1997).

The predominantly muddy sediments accumulating in the former tidal channels of the basin originate mainly from the River Rhine. Only in the southeastern part of the study area, near the outflow of the Meuse in the Hollandsch Diep, are the sediments dominated by Meuse River deposits. In the 1960s and 1970s, the suspended sediment from the Rhine and Meuse was severely polluted; since the 1980s, especially Rhine sediments have shown a significant

improvement in quality (Beurskens et al., 1994; Middelkoop, 1997). Throughout the study area, the heavily polluted ‘old’ sediments still surface locally in areas with low sedimentation rates, i.e. shallow near-shore areas and some deeper parts of the Haringvliet. Locations with high sedimentation rates, on the other hand, show less polluted recent deposits at the surface. The riverine sand settles out directly at the rivers’ entrance of the Hollandsch Diep (Van Dreumel, 1995, 1997; Van Wijngaarden, 1999). The sand found in the Haringvliet is a relict from the former estuarine situation; nowadays, no active sand deposition is found in the Haringvliet.

3. Fingerprinting

3.1. Sampling strategy

To obtain fingerprints, laboratory analyses of sediment samples were made. In March 1998, a first set of 12 sediment samples was taken from the top layer of the sediment in the Hollandsch Diep. Additional samples were taken during two MEDUSA field surveys: one in July 1998 for the Hollandsch Diep (ten

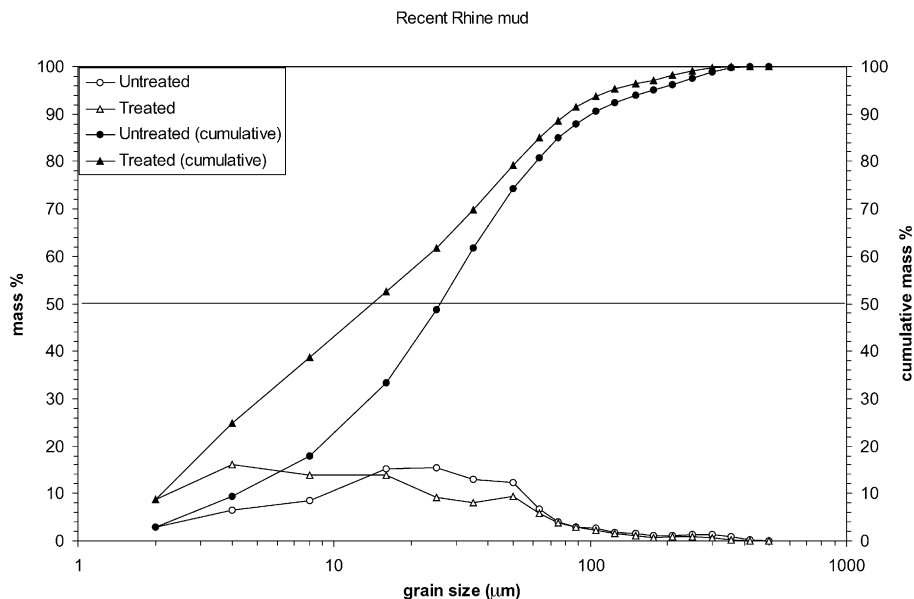


Fig. 4. Grain-size distribution of mud recently deposited by the Rhine.

samples) and one in August 1999 for the Haringvliet (17 samples). Knowledge of the main morphological features and sediment transport processes in the area formed the basis of each sampling cruise. A priori, it was not known how differences in provenance or age of the samples would affect the fingerprints of mud and sand. Therefore, in the first sampling round, special attention was paid to sampling sediment types with a different origin or age, which were considered to cover the majority of the surface sediment in the region:

1. Recent Rhine mud deposited during a period of improving suspended sediment quality (after 1980) (samples HD-A1/3).
2. Older Rhine mud deposited during the period of severe suspended sediment pollution in the period 1950–1980 (HD-A4/6).
3. Recently deposited Meuse mud (HD-A7/9).
4. Rhine sand (HD-A10/12).

The sampling locations are presented in Fig. 3; at each location, five samples were taken with a Van Veen

sediment grab, which samples the sediment top layer (about 20 cm).

The remaining samples presented in Fig. 3 were selected during two separate surveys in the Hollandsch Diep and the Haringvliet. The on-line MEDUSA output was used for selection, resulting in a choice of sampling locations with varying radionuclide composition. These samples were taken using a box corer, also sampling the top layer. In Fig. 3, these 10 Hollandsch Diep samples are specified by 'HD B-number' and the nine Haringvliet samples by 'HV-number'. Additionally, in the Haringvliet, scuba divers sampled sediment from directly under the sensor at eight locations; these samples are indicated by 'HV D-number' in Fig. 3. In this manner, three independent sets of samples were obtained, which were used for calibration and verification of the fingerprint.

3.2. Treatment of samples

All samples were dried and homogenised before radiometric and geochemical analysis. For the first set

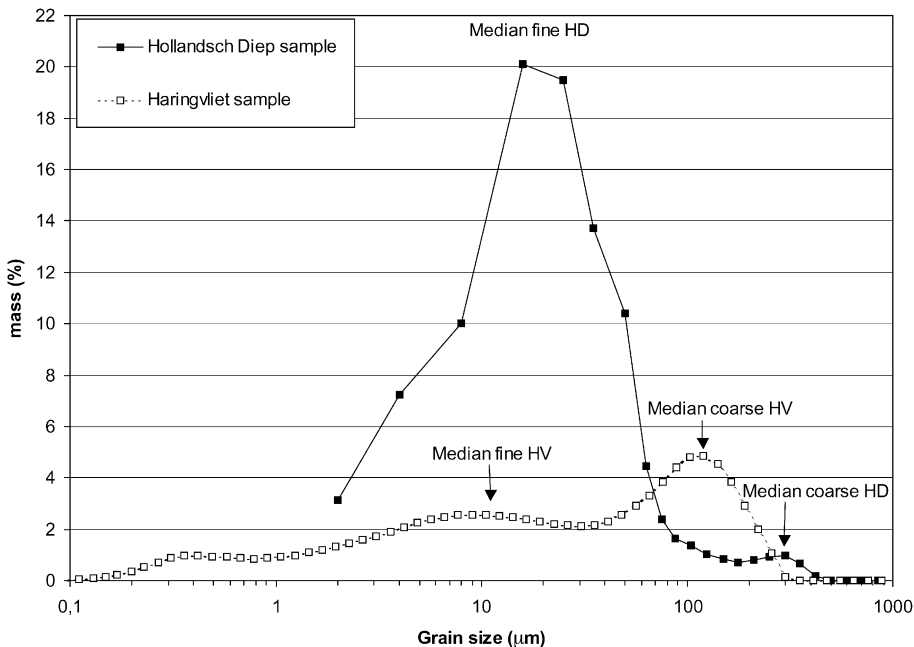


Fig. 5. A typical example of the grain-size distribution of a Haringvliet and Hollandsch Diep muddy sediment.

of samples (numbers 'A') from the Hollandsch Diep, an attempt was made to preserve the integrity of the samples and their radiometric characteristics by not pretreating them in any way. However, it turned out that aggregates from organic matter and clay minerals were bound together in aggregates $>63 \mu\text{m}$, thus erroneously contributing to the sand fraction. Consequently, all samples were pretreated with 30% H_2O_2 and 10% HCl , but only for the grain-size analysis. To preserve the radiometric and geochemical characteristics, pure and untreated samples were analysed.

3.3. Analytical techniques

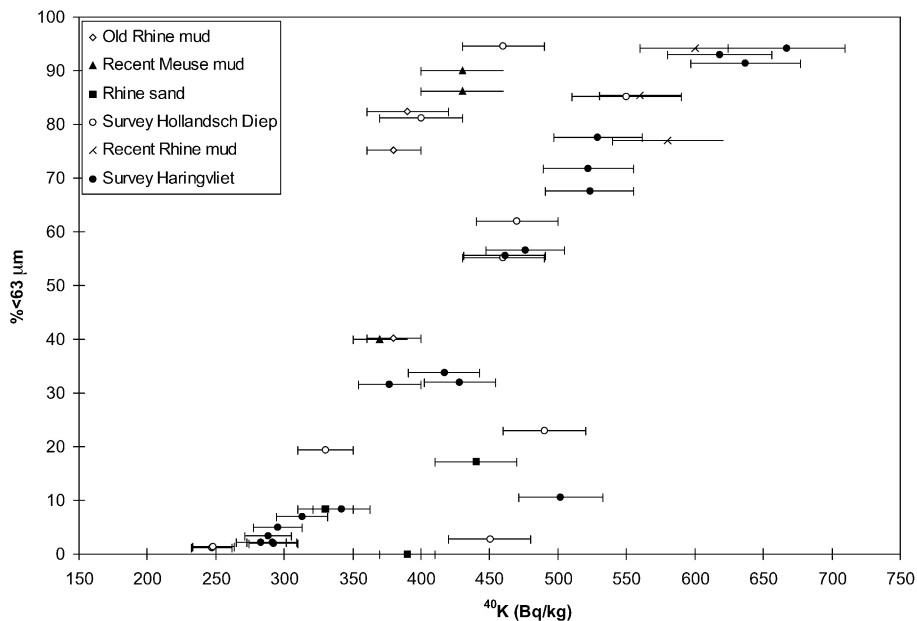
3.3.1. Grain-size determinations

Grain-size distributions were measured with a Malvern χ -mastersizer at NITG-TNO. Approximately 5 g of sample was put in an ultrasonic bath and the suspension was cycled through a measuring cell in front of the laser for 5 min. The correlation with sieving methods is good, with a systematic overestimation of d_{50} values for the laser method (Zonneveld, 1994; Konert and Vandenberghe, 1994).

3.3.2. Geochemical analysis

Total carbon and sulphur were measured with a Ströhlein CS-mat 5500 at NITG-TNO, by combustion of 0.1 g of sample at 1350°C while detecting the evading CO_2 and SO_2 by an infrared detector. Standard deviations are less than 5%. CaCO_3 was measured with a Ströhlein C-mat 5500 by CO_2 analysis after acidification with H_3PO_4 , using about 1 g of sample. Standard deviations are better than 5%. Organic carbon was calculated by subtracting calcite carbon from total carbon.

For XRF-analyses, 10 g of a sample was ground and subsequently pressed with wax into tablets. The tablets were analysed for major and trace elements by X-ray fluorescence spectroscopy, using an ARL8410 spectrometer at NITG-TNO, with full matrix correction for major elements and Compton scatter method for trace elements. The XRF was calibrated using approximately 100 certified geological reference samples. Three reference samples were added to each batch of 50 samples to determine precision (0.5–1% relative standard deviation) and accuracy (1–5% relative standard deviation).



3.3.3. Radiometric analysis

^{238}U and ^{232}Th are indirectly analysed using a few daughter radionuclides that emit γ -rays with sufficient intensity in the energy range of 0.1–2.6 MeV, essentially ^{214}Pb and ^{214}Bi for ^{238}U and ^{228}Ac and ^{208}Tl and ^{212}Pb for ^{232}Th . Escape of ^{222}Rn was prevented by sealing and, to restore the radiometric equilibrium, storage of the samples for a period of 3 weeks prior to measurement. Depending on the total volume of sample, samples were put in a re-entrant Marinelli beaker or in a small polystyrene box for an optimal geometry. The beaker or box was positioned on top of a high-purity germanium (HPGe) detector of NGD/KVI for γ -ray spectrometry. The HPGe detector is an EG and G Ortec p-type germanium detector, with crystal dimensions: $\Phi = 60.4$ mm, $h = 78.3$ mm. This is a general purpose, high-energy resolution instrument for measuring γ -rays with energies between 0.12 and 3 MeV. The detector is mounted inside a 10-cm lead shielding against room and cosmic ray background. The efficiency of the detector is calibrated with an aqueous solution of man-made radionuclides.

The efficiencies are corrected for matrix effects and for extra self-adsorption due to a sample density deviating from unity according to procedures outlined by Sima (1992).

In this investigation, activity concentrations of ^{40}K , ^{238}U , ^{232}Th and of the anthropogenic radionuclides ^{60}Co and ^{137}Cs were determined. The analysis of the γ -ray spectrum is based on the determination of the strength of photo peaks. The reported values of the series are the weighted averages for the activities for each γ -ray transition under the assumption of secular equilibrium (Evans, 1969) among the various decay products.

3.4. Assessment of fingerprints

The radiometric fingerprint of a sediment fraction is based on the assumption that the total activity concentration will be the sum of the activity concentrations from each fraction. This assumption seems to be valid since there are no physical processes to distort this linear relationship. The use of three radionuclides

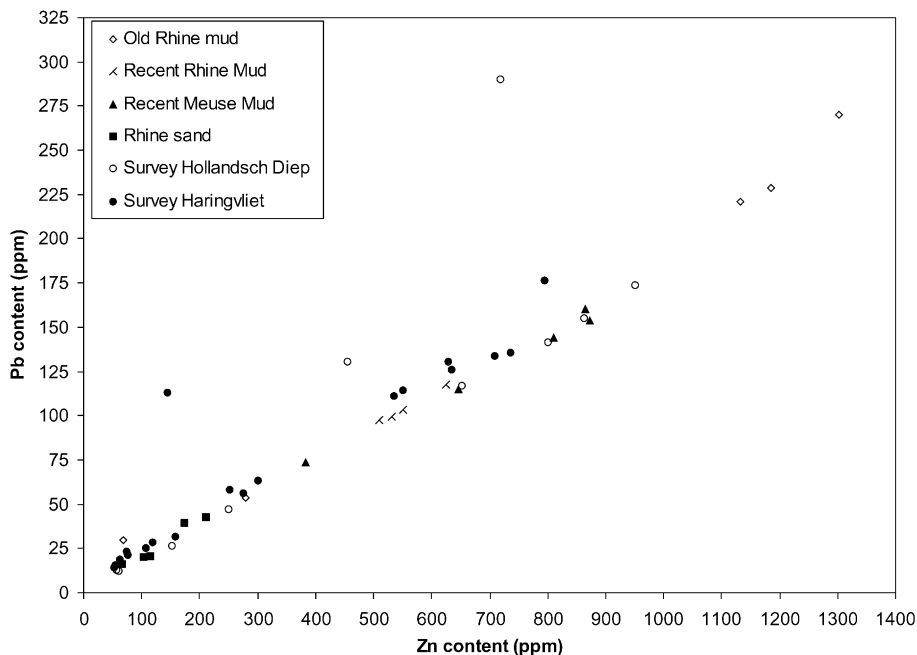


Fig. 7. Relation between the Pb content (ppm) and the Zn content (ppm) of all samples; the various sediment types are indicated by separate symbols.

allows the user to define a maximum of four sediment fractions, by solving the following set of equations:

$$m_{\text{fraction 1}} * C_{\text{fraction 1}}(\text{K}) + m_{\text{fraction 2}} * C_{\text{fraction 2}}(\text{K}) + m_{\text{fraction 3}} * C_{\text{fraction 3}}(\text{K}) + m_{\text{fraction 4}} * C_{\text{fraction 4}}(\text{K}) = C^{\text{tot}}(\text{K})$$

$$m_{\text{fraction 1}} * C_{\text{fraction 1}}(\text{U}) + m_{\text{fraction 2}} * C_{\text{fraction 2}}(\text{U}) + m_{\text{fraction 3}} * C_{\text{fraction 3}}(\text{U}) + m_{\text{fraction 4}} * C_{\text{fraction 4}}(\text{U}) = C^{\text{tot}}(\text{U})$$

$$m_{\text{fraction 1}} * C_{\text{fraction 1}}(\text{Th}) + m_{\text{fraction 2}} * C_{\text{fraction 2}}(\text{Th}) + m_{\text{fraction 3}} * C_{\text{fraction 3}}(\text{Th}) + m_{\text{fraction 4}} * C_{\text{fraction 4}}(\text{Th}) = C^{\text{tot}}(\text{Th})$$

$$m_{\text{fraction 1}} + m_{\text{fraction 2}} + m_{\text{fraction 3}} + m_{\text{fraction 4}} = 1$$

where: $m_{\text{fractions 1-4}}$ = the mass of the (four) sediment size fractions in the sample [-]; $C_{\text{fractions 1-4}}$ (K/U/

Th) = the activity concentration for each radionuclide in each sediment fraction of the sample [Bq/kg]; C^{tot} (K/U/Th) = the total activity concentration of the total sample for each radionuclide [Bq/kg].

The activity concentrations of the total sediment sample (C^{tot} (K), C^{tot} (Th), C^{tot} (U)) are known from radiometric analyses as are the mass fractions of mud and sand from grain-size analyses. With less than four sediment fractions, the set of equations will be over-determined. Since in the presented study, only two fractions, i.e. mud and sand, were distinguished, a least-squares procedure was used to determine the best possible solution obtained from matrix inversion.

4. Radiometric characterisation of the Rhine–Meuse sediments

Pretreatment with acids of samples prior to grain-size analyses resulted in two compensating effects: [1] destruction of relatively large organic aggregates and [2] destruction of the fine-grained material. The net effect on the d_{50} or the mud content depends on the composition of each sample. To illustrate this, in Fig.

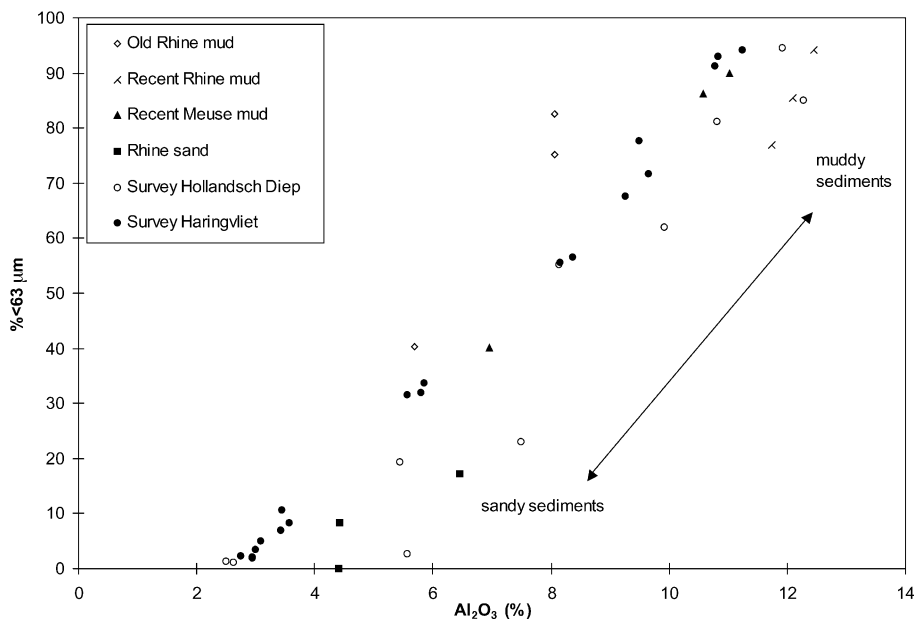


Fig. 8. Relation between the Al₂O₃ content (%) and the mud content (% < 63 μm) of all samples; the various sediment types are indicated by separate symbols.

4, the grain-size distributions of a muddy sample before and after treatment are presented, showing that treatment results in a decrease of the d_{50} of about 10 μm , whereas the mud content increases by several mass percents. Although the effect of treatment is observable, it turns out to hardly disturb the fingerprinting procedure.

Fig. 5 presents the grain-size distribution of a typical Hollandsch Diep and Haringvliet sample. The figure illustrates the general observation that Hollandsch Diep samples are muddier than Haringvliet samples. Moreover, as indicated in Fig. 5, in both samples, a fine and coarse fraction can be distinguished. For both samples, the mud fraction has a median diameter around 16 μm , whereas the sandy fraction contains particles with a diameter of 125 or 300 μm for the Haringvliet and Hollandsch Diep, respectively. This implies that the coarser sediment fraction becomes finer in the downstream direction; moreover, a higher proportion of the fine-grained fraction is found downstream.

The correlation between ^{40}K and mud appears to be rather poor ($R^2=0.57$, Fig. 6), which is due partly to differences in both provenance and age of the samples: relatively low values are found for the Meuse and old Rhine samples; both sample groups

are indicated in Fig. 6. The composition of the Meuse suspended matter confirms such low ^{40}K contents (Van Eck, 1982). Moreover, the high contents of organic matter and carbonate, which are components low in activity, may dilute the ^{40}K concentration in the old Rhine samples. The relation between the mud and ^{40}K content appears to be rather poor for the Hollandsch Diep ($R^2=0.38$) but strongly improved for the Haringvliet ($R^2=0.87$); see Figs. 9 and 10. In addition to the influence of old Rhine and Meuse mud, the presence of K-feldspars in the coarse fraction of some of the Hollandsch Diep samples has further deteriorated the relationship between ^{40}K and the mud content. These feldspars are deposited in the Hollandsch Diep and therefore do not play a role in the Haringvliet sediment. Moreover, all mudtypes will have been mixed during transport, making ^{40}K to correlate rather well with the mud content in the Haringvliet. Nonetheless, the use of ^{40}K for fingerprinting of mud and sand in this area should be handled with great consideration.

Since the old Rhine samples show deviant values for most analysed elements, a check on their age was needed for proper interpretation of the data (note that sampling was only based on expert-judgement). Heavy metal contents can be used as a tracer because

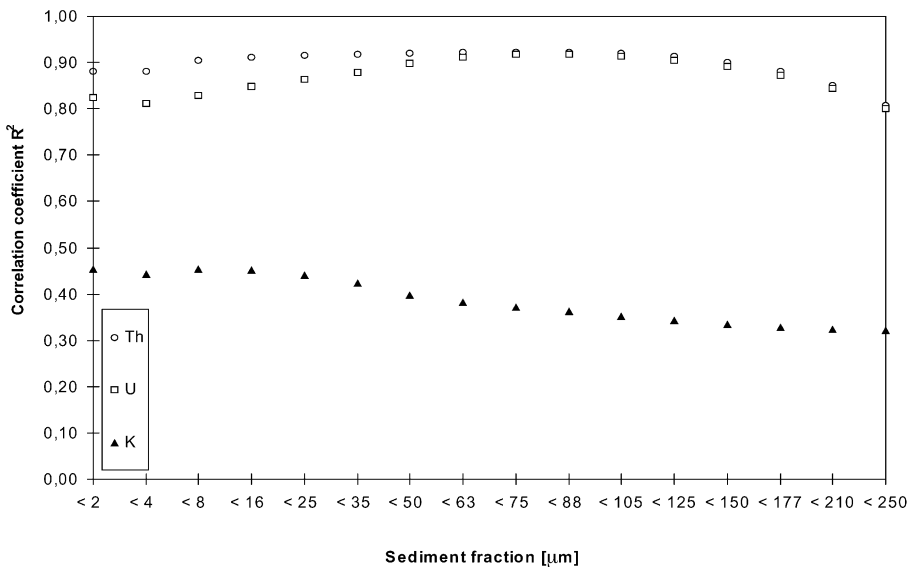


Fig. 9. Correlation among the ^{238}U , ^{232}Th and ^{40}K and sediment size fractions of <2 to 250 μm for the Hollandsch Diep samples.

from the pollution history of the Rhine, sediments deposited during the period 1950–1970 can be recognised by (extremely) high heavy metal contents (Beurskens et al., 1994; Middelkoop, 1997). In Fig. 7, the lead and zinc contents of all samples are presented, with the ‘old Rhine’ samples indeed having considerably high heavy metal contents. However, high organic matter, carbonate and sulphur contents in these samples indicate that diagenetic processes may also be partially responsible for these enhanced metal concentrations. Although these samples can definitely be considered ‘old’, it should be questioned how representative they are for the study area, given their atypical nature and secluded sampling locations.

The Al_2O_3 content of the samples is used to double-check the (diversity in) textural composition of the samples. In Fig. 8, the correlation between Al_2O_3 and the mud fraction is presented ($R^2=0.85$), which indeed shows high Al_2O_3 percentages (10–12%) for the samples with high mud contents and low percentages (3–7%) for the sandy samples. It was tested in the laboratory that the radiometric content of both organic matter and carbonates is much lower than that of the clay minerals. Although the presence

of such low activity components in muddy samples will dilute the total radiometric signal, this will only affect the fingerprint negatively if organic matter and carbonates are not evenly admixed to the mud fraction. The samples in this study showed no evidence of any effect on the fingerprint.

The question arises whether the division between mud and sand at $63\ \mu\text{m}$ is a reliable choice for fingerprinting. Therefore, the correlation coefficient of the regression between the measured radionuclide content and the amount of the fraction $<2\ \mu\text{m}$ up to the fraction $<250\ \mu\text{m}$ was assessed based on all samples. This correlation coefficient per sediment size fraction is presented for each of the radionuclides in Fig. 9 for the Hollandsch Diep samples and in Fig. 10 for the Haringvliet samples. Both figures illustrate that for both the Hollandsch Diep and Haringvliet, the correlation between ^{232}Th and ^{238}U is high ($R^2 \approx 0.8–0.9$) for sediment fractions up to $<100\ \mu\text{m}$. As has been pointed out before, ^{40}K only correlates well ($R^2 \approx 0.7$ to 0.8) in the Haringvliet samples and was left out of the fingerprint. Besides, these figures imply that the choice for a sediment fraction is more or less unrestricted in the range of fractions <2 to $100\ \mu\text{m}$;

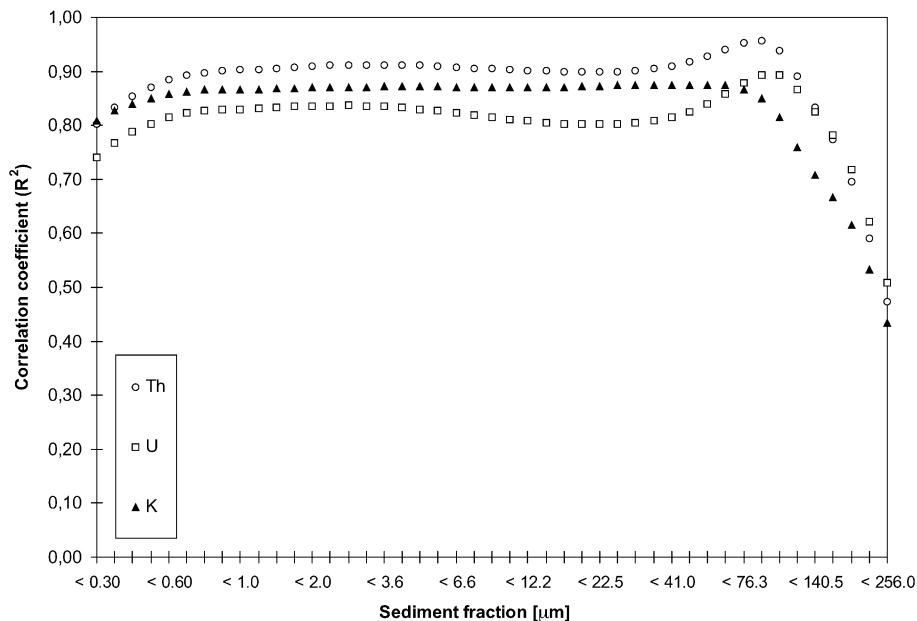


Fig. 10. Correlation between the ^{238}U , ^{232}Th and ^{40}K and sediment size fractions of <2 to $258\ \mu\text{m}$ for the Haringvliet samples.

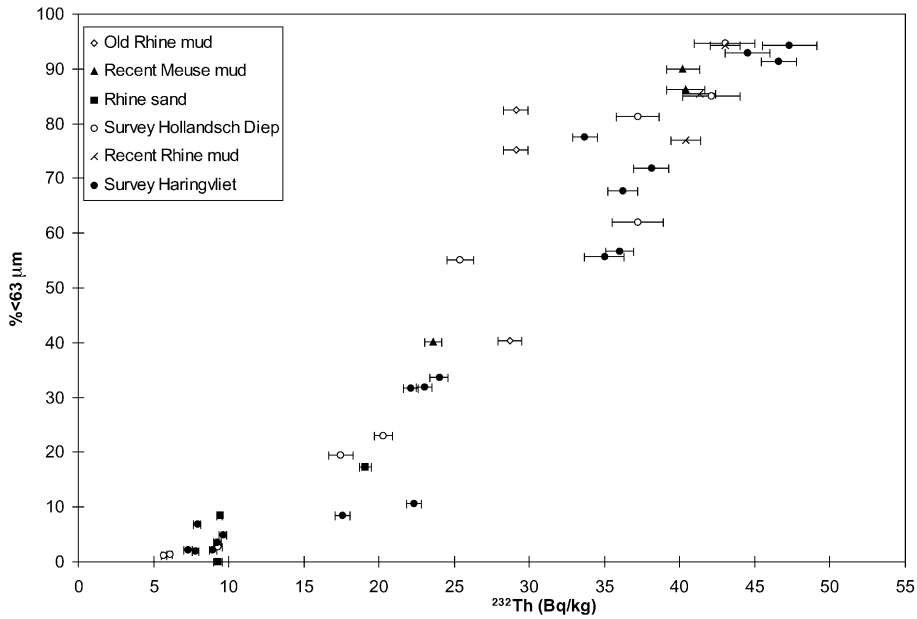


Fig. 11. Relation between the ²³²Th content (Bq/kg) and the mud content (%) of all samples; the various sediment types are indicated by separate symbols.

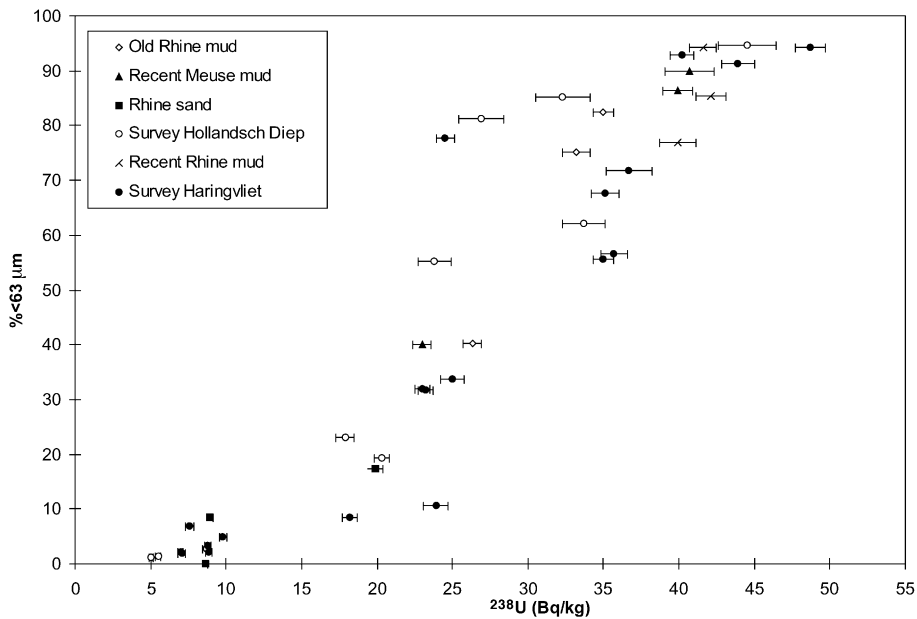


Fig. 12. Relation between the ²³⁸U content (Bq/kg) and the mud content (%) of all samples; the various sediment types are indicated by separate symbols.

Table 1

Characteristic radiometric fingerprints of sand and mud. The values are derived from the ^{238}U and ^{232}Th activity concentrations of untreated total samples

Sediment type	^{238}U -series (Bq/kg)	^{232}Th -series (Bq/kg)
Sand > 63 μm	9.3 ± 0.9	9.7 ± 0.9
Mud < 63 μm	46.2 ± 1.9	45.6 ± 1.9

the choice for the fraction < 63 μm in this study fits neatly within this range. For this mud fraction, the R^2 of the combined Hollandsch Diep and Haringvliet data equals 0.92 and 0.88 for ^{232}Th and ^{238}U , respectively.

The correlation between ^{238}U and ^{232}Th and mud is presented in Figs. 11 and 12. The muddy samples (fraction 63 μm > 60–70%) can be recognised by high activities (around 35–50 Bq/kg) and the sandy samples (fraction 63 μm < 20% to 30%) by low activities (around 5–25 Bq/kg). Although the correlation in both figures is strong, some scatter still exists. This

can be attributed to factors such as differences in mineralogical composition (provenance) or organic matter and carbonate content. For example, the two old Rhine samples show a relatively low ^{232}Th signal due to admixture of relatively high organic matter and carbonate contents. Nevertheless, such samples did not affect the reliability of the overall relationship. The fingerprint for the mud fraction is presented in Table 1.

The reliability of the fingerprints was examined by deriving the correlation between the measured sediment fraction (Malvern) and a calculated sediment fraction based on radiometry. The latter was calculated from the total $^{238}\text{U} + ^{232}\text{Th}$ activity of the samples using the fingerprint. The result is presented in Fig. 13; the negative values are due to uncertainties in the fingerprint evolving from grain-size analysis on pretreated samples and radiometric analysis on untreated samples. The estimated mud content (< 63 μm) with the fingerprint correlates well with those determined using the Malvern: correlation coefficient

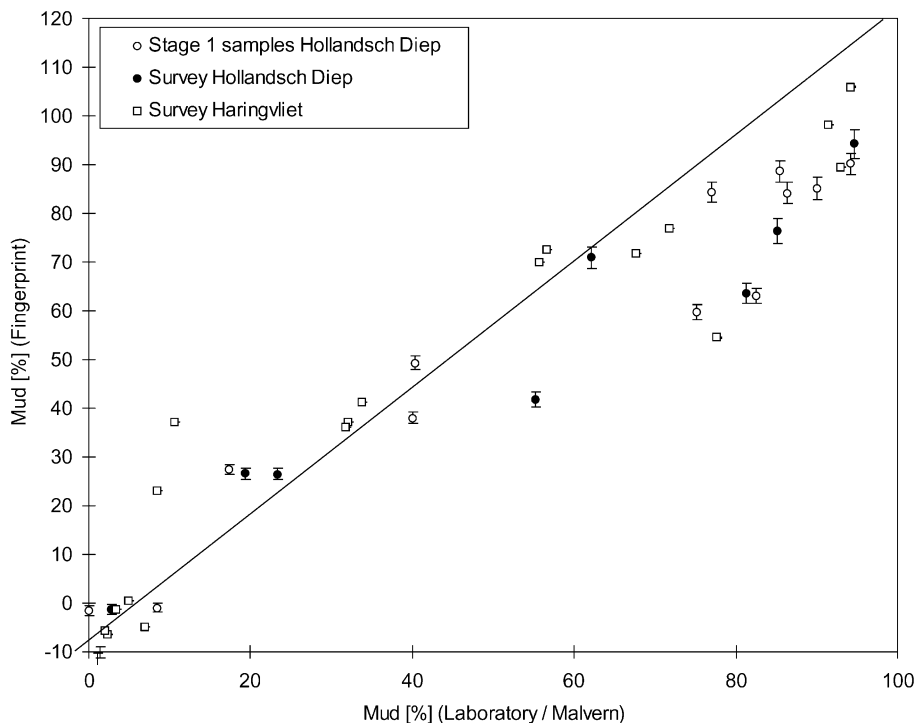


Fig. 13. Relation between the mud content (%) measured in the laboratory (Malvern) and the one evaluated from the activity of the total sample and the radiometric fingerprints of sand and mud.

$R^2 = 0.95$ and a root mean square error of 12%. From this correlation, it is not clear which of the two methods is more precise. Based on these results, one may conclude that sediments from the study area can successfully be characterised by radiometric fingerprinting.

5. Summary and conclusions

The goal of this study was to evaluate whether sediments can be characterised, in terms of mud and sand content, by their natural radionuclide content. Differences in age or origin were investigated using the geochemical and/or radiometric characteristic. Mud deposited by the Meuse shows a low ^{40}K signal, in agreement with the recent analysis of Meuse suspended matter. Moreover, mud deposited by the Rhine more than 50 years ago (Old Rhine mud) shows both low ^{40}K and ^{232}Th activity concentrations. This may be relative to their deviant composition, especially their high organic matter and carbonate contents. The presence of organic matter and carbonates will dilute the radionuclide activity concentration, but will affect the fingerprint only if they are not present in more or less uniform amounts to the mud fraction; the samples in this study however showed no evidence of such an effect on the fingerprint.

^{40}K was not used in the fingerprint since this did not correlate well with the fine fraction of the Hollandsch Diep samples. It turned out that the relationship between both ^{232}Th and ^{238}U with each sediment size fraction, ranging from fractions < 2 to $< 100 \mu\text{m}$, was excellent. The correlation between the mud fraction ($< 63 \mu\text{m}$) and ^{232}Th and ^{238}U yields an $R^2 = 0.92$ and 0.88 , respectively. Mud and sand were consequently characterised by $46.2 \pm 1.9 \text{ Bq/kg } ^{238}\text{U}$ and $9.3 \pm 0.9 \text{ Bq/kg } ^{238}\text{U}$ and $45.6 \pm 1.9 \text{ Bq/kg } ^{232}\text{Th}$ and $9.7 \pm 0.9 \text{ Bq/kg } ^{232}\text{Th}$, respectively. The accuracy of this fingerprint was tested independently against the Malvern grain-size analyses. The correlation between the mud fraction estimated by the fingerprint combined with the one measured by laser diffraction yielded an $R^2 = 0.96$, with a root mean square error of 12%.

It can be concluded that the activity concentrations of mud and sand differ by a factor of 5. Consequently,

radiometric fingerprinting offers a reliable way to determine the sand and mud content. The uncertainty in the radiometrically derived mud contents is small, in the order of 4–10%, supporting the conclusion that the radiometric signal and the mud content are closely related. Summarising, it can be concluded that radiometric sedimentology provides a tool for reliable sediment characterisation, which opens new perspectives in combination with the fast in situ radiometric characterisation of sediments by detector systems like MEDUSA. The application of this technique to the Rhine–Meuse estuary will be described in part B of this paper (this issue).

Acknowledgements

The authors wish to thank Mr. R. Ten Have and Mrs. H.P. Zwanenburg Nederlof for carrying out the radiometric and geochemical analyses.

References

- Beurskens, J.E.M., Winkels, H.J., De Wolf, J., Dekker, C.G.C., 1994. Trends of priority pollutants in the Rhine during the last fifty years. *Water Sci. Technol.* 29, 77–85.
- Duursma, E.K., Bosch, C.J., 1970. Theoretical, experimental and field studies concerning diffusion of radio isotopes in sediments and suspended particles of the sea: Part B. Methods and experiments. *Neth. J. Sea Res.* 4, 395–469.
- Duursma, E.K., Eisma, D., 1973. Theoretical, experimental and field studies concerning diffusion of radio isotopes in sediments and suspended particles of the sea: Part C. Applications to field studies. *Neth. J. Sea Res.* 6, 265–324.
- Evans, R.D., 1969. *The Atomic Nucleus*. McGraw-Hill, New York.
- Ferguson, H.A., Wolff, W.J., 1984. The Haringvliet project: the development of the Rhine–Meuse estuary from tidal inlet to stagnant fresh water lake. *Water Sci. Technol.* 16, 11–26.
- Hendriks, P.H.G.M., Limburg, J., De Meijer, R.J., 2001. *J. Environ. Radioact.* 53, 365–380.
- Horowitz, A.J., Elrick, K.A., 1987. The relation of stream sediment surface area, grain size and composition to trace element chemistry. *Appl. Geochem.* 2, 437–451.
- Konert, M., Vandenberghe, J., 1994. Comparison of laser grain-size analysis with pipette and sieve analysis. *Sedimentology* 44, 523–535.
- Middelkoop, H., 1997. Embanked floodplains in The Netherlands. Geomorphological evolution over various time scales. PhD thesis, University Utrecht.
- Sima, O., 1992. Photon attenuation for samples in Marinelli beaker geometry: an analytical computation. *Health Phys.* 62, 445–449.

- Van Dreumel, P.F., 1995. Zand en slib transport in het Noordelijk Deltabekken. Ministry of Transport, Public Works and Water Management, Directorate Southern Holland, Rotterdam.
- Van Dreumel, P.F., 1997. Het Noordelijk Deltabekken: metingen van zwevend stof transport en stroomsnelheid tijdens een hoge afvoer van de Rijn en Maas; Januari/Februari 1995. Ministry of Transport, Public Works and Water Management, Directorate Southern Holland, Rotterdam.
- Van Eck, G.T.M., 1982. De geochemie van het Hollandsch Diep en Haringvliet. PhD Thesis, University Utrecht, Netherlands.
- Van Eck, G.T.M., Zwolsman, J.J.G., Saeijs, H.L.F., 1997. Influence of compartmentization on the water quality of reservoirs: lessons learned from the enclosure of the Haringvliet estuary, The Netherlands. Proceedings of the Dix-neuvieme Congres des Grand Barrages, Florence, pp. 647–669.
- Van Wijngaarden, M., 1999. A two dimensional model for suspended sediment transport in the Rhine–Meuse estuary (The Netherlands). *Earth Surf. Processes Landforms* 24, 1173–1188.
- Van Wijngaarden, M., Ludikhuizen, D., 1997. Morfologie en sediment kwaliteit in het Noordelijk Deltabekken; MER Haringvlietsluizen, RWS report 98.094.
- Venema, L.B., De Meijer, R.J., 2001. Natural radionuclides as tracers of the dispersal of dredge spoil dumped at sea. *J. Environ. Radioact.* 55 (3), 221–239.
- Zonneveld, P.C., 1994. Vergelijkend onderzoek korrelgroottebepaling (zeef/Malvern). Report OP6500, Dutch Geological Survey.
- Zwolsman, J.J.G., Van Eck, G.T.M., Burger, G., 1996. Spatial and temporal distribution of trace metals in sediment from the Scheldt Estuary, south-west Netherlands. *Estuarine Coastal Shelf Sci.* 43, 55–79.